A simple theory of molecular organization in fullerene-containing liquid crystals

S. D. Peroukidis, A. G. Vanakaras,[a] and D. J. Photinos
Department of Materials Science, University of Patras, Patras 26504, Greece

(Received 22 June 2005; accepted 31 August 2005; published online 25 October 2005)

Systematic efforts to synthesize fullerene-containing liquid crystals have produced a variety of successful model compounds. We present a simple molecular theory, based on the interconverting shape approach [Vanakaras and Photinos, J. Mater. Chem. **15**, 2002 (2005)], that relates the self-organization observed in these systems to their molecular structure. The interactions are modeled by dividing each molecule into a number of submolecular blocks to which specific interactions are assigned. Three types of blocks are introduced, corresponding to fullerene units, mesogenic units, and nonmesogenic linkage units. The blocks are constrained to move on a cubic three-dimensional lattice and molecular flexibility is allowed by retaining a number of representative conformations within the block representation of the molecule. Calculations are presented for a variety of molecular architectures including twin mesogenic branch monoadducts of C_{60}, twin dendromesogenic branch monoadducts, and conical (badminton shuttlecock) multiadducts of C_{60}. The dependence of the phase diagrams on the interaction parameters is explored. In spite of its many simplifications and the minimal molecular modeling used (three types of chemically distinct submolecular blocks with only repulsive interactions), the theory accounts remarkably well for the phase behavior of these systems. © *2005 American Institute of Physics*.
[DOI: 10.1063/1.2085026]

I. INTRODUCTION

The possibility of controllable formation of ordered molecular assemblies of fullerenes is of fundamental importance for the use of these allotropes in applications.[1–3] However, the strong interactions among fullerene molecules normally lead to the formation of aggregates and therefore addends are used in order to modify favorably these interactions. The covalent linkage of fullerenes to liquid-crystal (LC) forming molecules (mesogens) offers a way to self-organized structures in which the fullerenes form ordered molecular assemblies.[4] Viewed from the LC perspective, the fullerination of mesogens establishes a new direction in the design of mesomorphic functional materials, given the peculiar photo- and electrochemical properties of the fullerene molecule.

Starting in 1996 with the work of Chuard and Deschenaux,[5] systematic efforts to synthesize fullerene-containing LCs have produced a variety of successful model compounds. These compounds are formed by the covalent linkage of one or more mesogenic units, typically of the calamitic (rodlike) type, at one or more sites of the fullerene frame. Depending on the structure of the mesogenic part and the topology of the fullerene-mesogen linkage, these compounds can be grouped into the following types, with the respective architectures illustrated in Fig. 1.

(a) Twin mesogenic branch monoadducts[4–9] of C_{60} in which two branches are attached, typically via a methanofullerene connecting group. The branches start out with a flexible alkyl spacer and terminate with a rodlike mesogenic unit [Fig. 1(a)]. Compounds of this type have been reported to form exclusively smectic-*A* mesophases.

(b) Twin dendritic branch monoadducts[6–8,10–12] of C_{60}, with two branches, as in (a), except that each branch is linked to a whole dendrimer [Fig. 1(b)], the branches of which are functionalized with mesogenic units (dendromesogen). The dominant LC phase exhibited by these supermesogens is the smectic-*A* mesophase, although the possibility of formation of nematic phases, in addition to the smectic-*A* phase, has been reported for certain low-generation denromesogen addends.[7,12]

(c) Single dendromesogenic branch monoadducts[7,8,13,14] of C_{60}. These are modifications of (b) in which one of the two branches terminates in a dendromesogenic unit and the other has a nondendritic terminus [Fig. 1(c)]. These compounds are reported to exhibit smectic-*A* mesophases.

(d) Dendromesogenic bisadducts[15] of C_{60} [Fig. 1(d)] with two dendromesogenic branches as in (b). The structure of the mesophase formed by these compounds has not been identified conclusively.

(e) Mesogenic branch hexa-adducts[16] of C_{60}. Six pairs of twin branches, each bearing a terminal mesogenic part, are attached via six methanofullerene connecting groups [Fig. 1(e)]. These supermesogens form smectic-*A* phases.

(f) Conical (badminton shuttlecock) multiadducts[17–19] of C_{60} [Fig. 1(f)]. The conical surface is formed by the direct attachment of (five) mesogenic units via single bonds to carbon sites of the fullerene, which thus be-

[a]Electronic mail: vanakara@upatras.gr

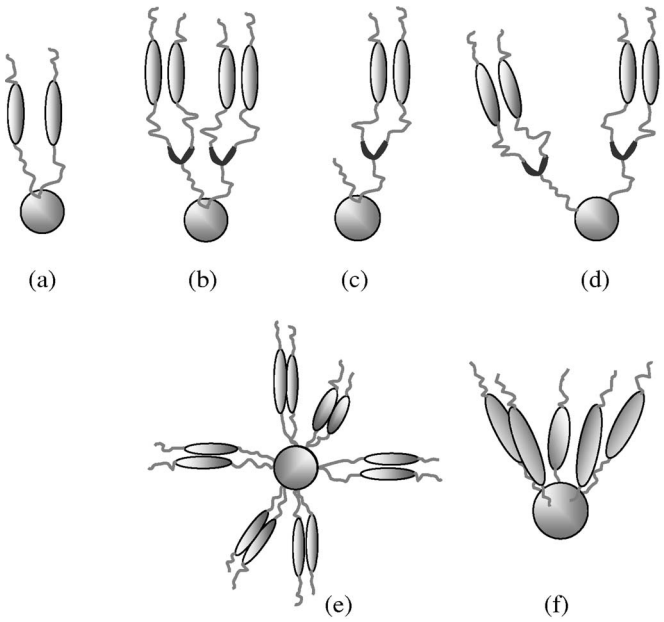

FIG. 1. Various architectures of mesogen-functionalized fullerenes: (a)–(c) monoadducts, (d) bisadducts, (e) hexa-adducts, and (f) conical multiadducts of C_{60}.

comes the apex of the cone. Hexagonal- and nematic-columnar mesophases have been reported for these supermesogens.

The variety of fullerene-containing LC compounds is already broad enough to permit the deduction of certain trends and possibly empirical design rules and also to provide testing grounds for a molecular theory. The purpose of this paper is to introduce a simple molecular theory relating the self-organization exhibited by these systems to their molecular structure.

The molecular interactions are modeled in a modular fashion. The fullerene-containing mesogen is divided into a number of chemically distinct submolecular components (modules) to which specific interactions are assigned. The total interaction of the molecular ensemble is then built up as a combination of interactions between all the possible pairs of modules within the ensemble. To simplify the computational aspects of the theory, the modular subdivision of the molecules is done rather coarsely, distinguishing only three types of submolecular components: fullerene units, mesogenic units, and nonmesogenic units (flexible spacers and linkage groups). For the same reasons of simplicity, the molecules are taken to move on a cubic three-dimensional lattice.

In its present primitive form, the theory attempts to describe in a unified way only the basic trends observed in the self-organization of these systems. It is not intended to provide a quantitative description or to account for peculiarities. Indeed, it is well known from the study of many conventional "simple" LCs that apparently small changes in the molecular structure could bring about dramatic changes in the self-organization. The treatment of analogous situations in fullerenated LCs is clearly beyond the reach of the present form of the theory.

The modeling of the molecular conformations and interactions is described in Sec. II. The results of the calculations for various architectures of fullerenated LCs are presented and their significance is discussed in Sec. III. The conclusions from this work are stated in Sec. IV. An appendix is included for completeness where the statistical-mechanics formulation underlying the phase-transition calculations is outlined.

II. MOLECULAR MODELING ON A CUBIC LATTICE

The statistical-mechanics machinery of the present theory is based on the interconverting shape approach[20] and summarized in the Appendix. In this section we describe the application of this approach to study the phase behavior of fullerene containing supermesogens of various architectures. As detailed in Ref. 20, the necessary ingredients for the implementation of this approach are as follows.

(i) The identification of a number of discrete molecular states or "shapes" representing the basic types of molecular conformations.
(ii) The assignment of an intrinsic probability P_S^0 to each shape S, giving the probability of finding an *isolated* molecule in that shape. Equivalently, an intrinsic free energy ε_S is assigned to each of these shapes.
(iii) The coarse-grained subdivision of the molecules into blocks with specified interactions. The overall molecular interactions are then described by a modular pair potential combining the interactions among all possible intermolecular pairs of blocks.

These ingredients are molecular characteristics that can be obtained to the desired detail by standard molecular-mechanics calculations on the atomistic scale. However, as the focus of this work is on the qualitative picture of mesophase description, rather than on quantitative accuracy, a minimal number of representative molecular shapes will be introduced, with rough estimates for their intrinsic probabilities, and a rather coarse molecular subdivision will be used together with a very simple parametrization of the block-block interactions. Thus, based on the presence of the fullerene molecule in the systems presented in Fig. 1, we have chosen to model their chemical structures on the length scale of the diameter of a single fullerene. An analogous discretization, on that length scale, is applied to the molecular motions in space. The molecules are constrained to move on a rectangular three-dimensional lattice with unit-cell dimensions equal to a fullerene diameter. The coarse-grained molecular shapes are then tailored using building blocks of size equal to the unit cell of the lattice space. In all cases considered here the molecular states consist of a building block corresponding to the fullerene unit and of several blocks connected to build up the grafted addends according to the molecular architecture of the state. Block representations for selected molecular architectures from Fig. 1 are depicted in Figs. 2–4.

Once the molecular shapes have been built, the interac-

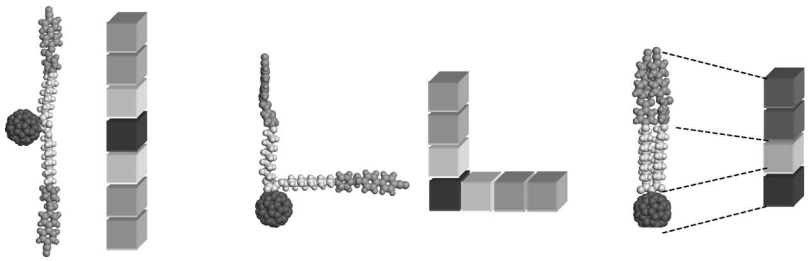

FIG. 2. Space filling and block representations of the dominant shapes of typical monoadduct C_{60} derivatives. Darker shading in the three top blocks in (c) is used to indicate coincidence of two blocks within a single lattice site.

tion potential $U_{I,J}$ between molecules I and J is obtained in a modular fashion[20] by combining interaction contributions among intermolecular pairs of blocks,

$$U_{I,J} = \sum_{b_I,b_J} (\boldsymbol{u}^{(0)}_{b_I,b_J}\delta(\boldsymbol{R}_{b_I,b_J}) + \boldsymbol{u}^{(1)}_{b_I,b_J}\delta(|\boldsymbol{R}_{b_I,b_J}| - 1)), \quad (1)$$

where $\boldsymbol{R}_{b_I,b_J}$ denotes the distance between blocks b_I and b_J, and $\boldsymbol{u}^{(0)}_{b_I,b_J}$ and $\boldsymbol{u}^{(1)}_{b_I,b_J}$ stand for the interaction potentials for a pair of blocks occupying the same or adjacent lattice sites, respectively. In what follows the block index b can be either f or m or l, denoting, respectively, fullerene units, mesogenic units, and nonmesogenic linkage units. We assume the following general form for the intermolecular block-block interaction potential $\boldsymbol{u}^{(n)}_{b_I,b_J}$, $n=0$, 1:

$$\boldsymbol{u}^{(n)}_{b,b'} = q^{(n)}_{b,b'} + w^{(n)}_{b,b'}P_2(\mathbf{e}_b \cdot \mathbf{e}_{b'}), \quad (2)$$

with $q^{(n)}_{b,b'}$ and $w^{(n)}_{b,b'}$ being strength parameters for the interactions among blocks b and b' when they occupy the same, $n=0$, or adjacent, $n=1$, cells.

The $q^{(n)}_{b,b'}$ terms define the strength of the nondirectional (isotropic) part of the block-block interactions. It should be noted, however, that these terms alone are sufficient to generate a directionality in the *overall interaction* among the molecules if the (nondirectional) blocks are connected together in a directional manner (as it is the case in all the block representations of the shapes in Figs. 2–4. The terms $w^{(n)}_{b,b'}$ in Eq. (2) allow for the inclusion of intrinsic directionality in the block-block interactions. This would account for the anisotropic interactions among mesogenic units, in the case where blocks b and b' correspond to such units. The directionality is conveyed simply by the Legendre polynomial of second order, $P_2(\mathbf{e}_b \cdot \mathbf{e}_{b'})$, where $\mathbf{e}_b$ and $\mathbf{e}_{b'}$ are unit vectors defining the long axes of the mesogenic units. In the block constructions used here (Figs. 2–4), these axes coincide with the directions of the branches to which the mesogenic units belong. Polar interactions among blocks have been ignored but they could readily be accounted for in more elaborate calculations by including $P_1(\mathbf{e}_b \cdot \mathbf{e}_{b'})$ terms in Eq. (2). Their omission from the present calculations is done for reasons of simplicity and does not necessarily imply that their effects are negligible. In fact, the molecular structures of most of the compounds considered in this study include segments with strong electric dipole moments and such moments are known to affect significantly the relative stability of liquid-crystalline phases of common mesogens.[21,22]

Next, we describe in some detail the conformation structure and intrinsic probabilities as well as the block idealization and interactions for three generic architectures of fullerene-containing supermesogens.

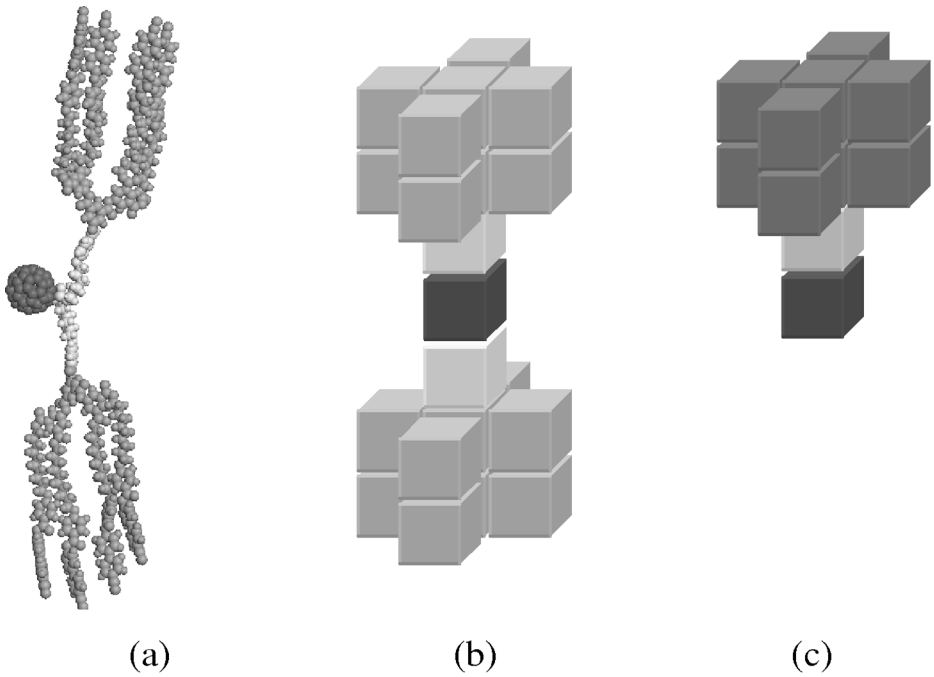

FIG. 3. Space-filling model (a) and block representations of two representative shapes, (b) and (c), of a typical 2nd generation dendritic monoadduct C_{60} derivative. Darker shading in all but the bottom block the in (c) is used to indicate coincidence of two blocks within a single lattice site.

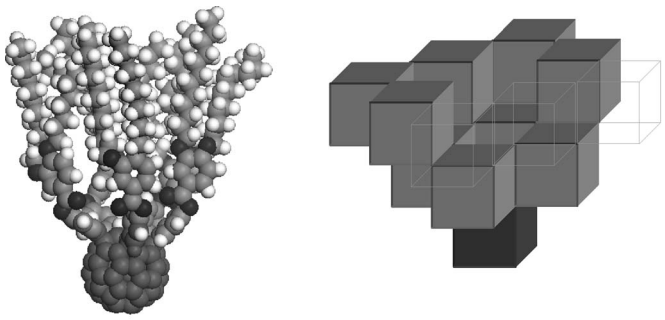

FIG. 4. Space-filling model (a) and block representation (b) of a multiadduct fullerene derivative with conical shape. The wire-frame drawing of some blocks has been used in order to provide a better view of the empty space between the grafted addends.

A. Twin mesogenic branch of C_{60}(TMB-C_{60})

These consist of two identical branches grafted on the surface of a C_{60} fullerene, Fig. 1(a), with each branch bearing one mesogenic unit. Clearly, the number of accessible conformations for such systems is quite large due to the flexibility of the spacers connecting the C_{60} moiety with the mesogenic units. Furthermore, molecular-mechanics calculations with widely accepted empirical force fields[23] indicate that conformations of completely different overall shapes may not differ substantially in their energies. In addition, molecular states with the mesogenic units on the same side of the C_{60} and mutually parallel, despite some energetic gain due to van der Walls attractions between the mesogenic units (compared to states with the mesogenic units far apart), are achieved for a limited number of energetically accessible conformations of the flexible spacers and thus become entropically disfavored.

Based on these considerations we model the TMB-C_{60} systems by grouping the molecular conformations in three distinct coarse-grained molecular shapes. Each shape consists of a single fullerene block and two branches. With building blocks of the fullerene size, the actual length of each branch is roughly three times the fullerene diameter. Consequently, each branch consists of three linearly attached building blocks of which the one closest to the fullerene is partially occupied by the flexible spacer and the next two are occupied by the mesogenic unit. In the first of the shapes, to be referred to as the extended antiparallel (EA) shape (denoted by EA), the two branches extend in opposite directions rendering the shape cylindrical symmetric (strictly, fourfold symmetric on the cubic lattice) and apolar [Fig. 2(a)]. In the second, the L shape (denoted by L), the two branches are mutually perpendicular and the molecular shape lacks both, apolarity and cylindrical symmetry [Fig. 2(b)]. In the third shape, to be referred to as the folded parallel (FP) shape (denoted by FP) both branches share the same space [Fig. 2(c)] and the molecular block representation is cylindrically symmetric and polar.

With each branch constrained to a linear array of the building blocks, these three shapes exhaust all the possibilities on a cubic lattice. Accordingly, the various bent (V-shaped) conformations, which represent the majority of the TMB-C_{60} molecular states, are understood to be conveyed by one of these shapes, depending on the magnitude of the bent angle (the FP shape for acute bend, the EA shape for flight bend, and the L shape for intermediate bend angles).

For this class of systems the branches grafted on the fullerene are not very bulky. Hence we assume that any two submolecular blocks interact only when they occupy the same lattice site and consequently $u^{(1)}_{b,b'}$ of Eq. (1) is taken to vanish for any pair of blocks. For the parametrization of $u^{(0)}_{b,b'}$ we assume that the lattice sites containing fullerene building blocks are not permitted to be occupied by any other block, i.e., fullerene blocks are impenetrable both to other fullerene blocks and to blocks corresponding to branches. Furthermore, the building blocks of the branches are assumed to exert on one another soft repulsions without any directionality. In the parametrization of Eq. (2), these assumptions correspond to $w^{(0)}_{b,b'}=0$ for any intermolecular pair of blocks b,b', $q^{(0)}_{f,b}=\infty$ for $b=f$ or m or l, and $q^{(0)}_{l,l}=q^{(0)}_{m,m}=q^{(0)}_{l,m}=u>0$, with u serving as the measure of the "hardness" of the repulsive interactions among these blocks. The implications on the molecular organization of the TMB-C_{60} upon the inclusion of directional interactions between branches are also considered in some of our calculations by allowing for $w^{(0)}_{b,b'}\neq 0$.

The intrinsic free energies of the shapes with extended antiparallel or perpendicular branches are assumed to be equal, $\varepsilon_{\mathrm{EA}}=\varepsilon_L=0$. For the intrinsic free energy $\varepsilon_{\mathrm{FP}}$ of the remaining, FP, shape we consider the three possibilities $\varepsilon_{\mathrm{FP}}>0$, $\varepsilon_{\mathrm{FP}}=0$, or $\varepsilon_{\mathrm{FP}}<0$ corresponding to this shape being intrinsically less, equal, or more probable than the other two shapes.

B. Twin dendromesogenic branch of C_{60}(TDB-C_{60})

This is the case of liquid-crystalline dendrons attached to the C_{60} surface giving rise to molecular architectures similar to those in Figs. 1(b) and 1(d) and their higher generation counterparts. The chemical structure of a second generation mesogenic dendrimer grafted at a single point on the fullerene surface[7,8] is depicted in its fully extended conformation (the two dendritic branches extending in opposite directions) in Fig. 3(a). In accordance with molecular-mechanics calculations, conformations with both dendritic branches on the same side of the fullerene (not shown in Fig. 3) are also possible. Therefore we assume that the molecular conformations can be grouped in two dominant molecular shapes with the dendritic units extending either on the same side (FP shape) or to the opposite sides (EA shape) and we have built these shapes according to the shapes shown in Figs. 3(b) and 3(c). At this level of resolution, the primary difference from the structures of Fig. 2 is that the arms grafted to the fullerene are bulkier. Different tones of shading have been used in Fig. 3 to distinguish blocks of different contents. We have used the darker shading for the addends of the FP shape to indicate that, in this case, the addend blocks of both branches share the same space and therefore their density is twice as large compared to the density of the corresponding blocks of the EA shape.

TABLE I. Interaction parameters for building blocks occupying the same lattice site, $q^{(0)}_{b_1,b_2}$, or adjacent lattice sites, $q^{(1)}_{b_1,b_2}$ (values in brackets).

b_1 / b_2	$f(C_{60})$	l (Spacer)	m (Mesogens)
$f(C_{60})$	∞ (0)	$\infty(u/2)$	$\infty(u/4)$
l (Spacer)	$\infty(u/2)$	$u(u/4)$	$u/4$ (0)
m (Mesogens)	$\infty(u/4)$	$u/4$ (0)	$u/4(u/8)$

Calculations were performed initially with the inclusion of a third, L, shape. These calculations showed, however, that the inclusion of this shape does not alter significantly the phase behavior of the system. The parametrization of the block-block interactions when the blocks occupy the same lattice site is similar to the corresponding parametrization for the TMB-C_{60} blocks. In order to convey the bulkier nature of the dendritic addends of the TDB-C_{60} we have assumed that the addend blocks repel softly each other even when they are in adjacent cells. The form of the interaction potential we have used for the calculations for the block model of TDB-C_{60} is summarized in Table I where the single hardness parameter u corresponds to the strength of the repulsive potential between two l blocks when they occupy the same lattice site.

It should be noted here that this block representation is expected to break down for grafted dendromesogens of generation higher than the third. In that case, the fullerene size becomes very small compared to the rather bulky branches which would thus cover the fullerenes completely, therefore preventing any direct fullerene-fullerene interactions.

C. Conical supermesogens with a fullerene apex (CSM-C_{60})

These are shown in Fig. 4 together with the respective block structure used in the present modeling. Here we assume two kinds of molecular building blocks, the fullerene blocks (f blocks) and the blocks that correspond to the grafted addends (m blocks). A single shape is assumed for these systems. This renders the block representation of the supermesogen rigid. Such representation is in line with the chemical structures of the CSM-C_{60} where five aromatic groups are attached around a pentagon of the fullerene molecule[17–19] thus forming an essentially rigid "nanoshuttlecock." Certainly, the presence of aliphatic end chains on the grafted mesogenic groups of the real systems introduces some molecular flexibility which, however, entails only minor deviations from the dominant hollow-cone molecular shape.

For a broader assessment of the significance of the results to be presented in the next section, it is worth noting that, first, the theoretical framework outlined here is not restricted to fullerene containing LCs nor is the lattice representation an inherently restricting feature of the theory; it merely reduces the computational effort without seriously distorting the essence of the molecular description. Secondly, the assignment of the *interblock* interactions adopted here is based mainly on intuition. However, taking into account the detailed structure of chemical units that fill the building blocks, the use of simple molecular-mechanics calculations can provide more accurate estimates of the interblock interactions.

III. RESULTS AND DISCUSSION

Here we present results on the phase behavior of the three types of model structures introduced in the previous section. Starting with the TMB systems, different situations are explored within the parametrization adopted for the block-block interactions (strength parameter u) and the intrinsic probabilities of the molecular conformations (parameter ε_{FP}). For all the combinations of u and ε_{FP} studied, the mesophases formed by these systems are nematic and orthogonal smectic phases of different layer structures.

Due to the possibility of interconversions between molecular states of significantly different molecular lengths, the smectic polymorphism found in these systems has some notable differences from the polymorphism of conventional smectic compounds for which a single molecular length is dominant. It is known that strongly polar rodlike molecules give rise to a rich polymorphism of orthogonal layered mesophases.[22,24–26] Thus, distinctions of the smectic-A (SmA) phases into SmA_1, SmA_d, and SmA_2 phases are introduced, where the indices 1, d, and 2 indicate that the wavelength of the periodic density modulation is, respectively, one, $d(1<d<2)$ or two times the effective molecular length. Moreover, incommensurate SmA_i phases have been reported.[26] These phases are characterized by spatial modulations along the nematic director with wavelengths ℓ and ℓ' of irrational ℓ/ℓ' ratio. This classification of the smectic-A phases assumes the existence of a single molecular length (or at least a narrowly defined range of molecular lengths). Clearly this is not the case for the TMB systems of Fig. 2 where the three dominant states of the molecule are vastly different in their geometrical characteristics. However, for the purpose of the present study we have labeled the smectic phases in close analogy to the widely accepted nomenclature of the conventional smectic compounds, by defining the "molecular length" to be the sum of the grafted branch length and the fullerene diameter. According to this choice of molecular length measure, we denote by SmA_{d1} highly interdigitated smectic phases where the fullerenes within a smectic layer form a single sublayer of thickness equal to the fullerene diameter (fullerene monolayer). Smectic-A structures with a structure similar to SmA_{d1} but with the thickness of the fullerene-rich sublayers being twice the fullerene diameter are denoted as SmA_{d2} (fullerene bilayer within a single smectic layer). Finally, incommensurate smectic phases with structures corresponding to a superposition of SmA_{d1} and SmA_{d2} are denoted as SmA_{di}.

The phase behavior of the TMB systems, adopting the above nomenclature for the layered phases, is summarized in Figs. 5(a)–5(d) where we plot pressure versus reciprocal temperature phase diagrams for various values of the scaled intrinsic free-energy difference ε_{FP}/u. In all cases, the systems exhibit an isotropic phase (I), different orthogonal smectic phases, and a low-temperature uniaxial nematic phase (N) which, however, is stable over a rather narrow

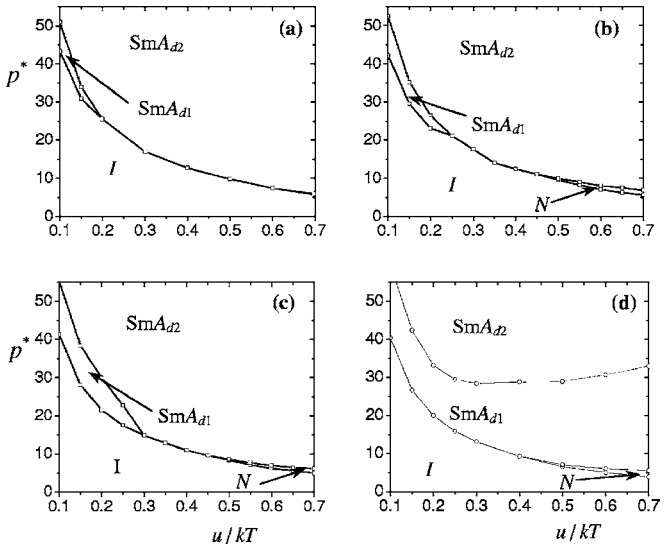

FIG. 5. Calculated phase diagrams (scaled pressure vs reciprocal temperature) for the three state interconverting model of the TMB-C_{60} monoadducts. The EA and L shapes have been taken to have equal intrinsic probabilities ($\varepsilon_{EA}=\varepsilon_{L}=0$) and four different cases for the intrinsic probability of the third, FP, shape were considered corresponding to: (a) $\varepsilon_{FP}/u=-3$, (b) $\varepsilon_{FP}/u=-1$, (c) $\varepsilon_{FP}/u=1$, and (d) $\varepsilon_{FP}/u=3$. The interaction parameter q_0 has been set equal to 0.1 in all cases.

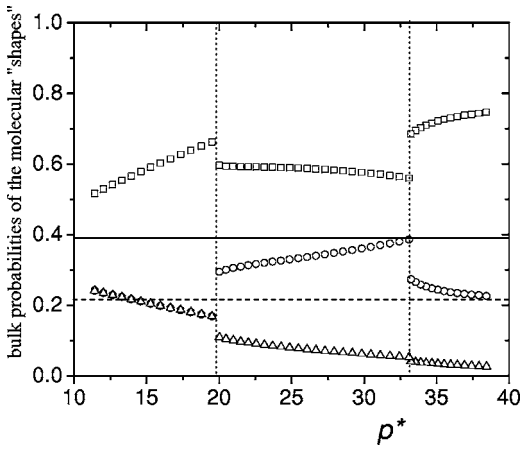

FIG. 6. Calculated bulk probability of the EA (circles), the L (triangles), and the FP (squares) shapes, as a function of pressure for the system whose phase diagram is given in Fig. 5(c) at the fixed value of scaled temperature $u/k_BT=0.2$. Shown on the diagram are also the intrinsic probabilities of the EA and L shapes (solid line) and of the FP shape (dashed line).

region of the phase diagram [not shown at all within the plotted temperature range in Fig. 5(a)]. The orthogonal smectic phases differ in the way the fullerenes organize within the smectic layers and also in the degree of interdigitation of the arms in adjacent smectic layers. Specifically, in the high-temperature, high-pressure smectic phases the fullerenes are arranged on a single sublayer (fullerene monolayer, SmA_{d1}) while in the lower-temperature smectic phases the fullerenes occupy two successive sublayers (fullerene bilayer, SmA_{d2}).

All the phase transitions are of first order. The SmA_{d1}-SmA_{d2} and the isotropic to nematic transitions are weaker than the isotropic to smectic transitions and nematic to smectic transitions. The nematic phase, for all the studied systems, appears only at low temperatures where the shapes become practically impenetrable and their self-organization is determined primarily by the overall shape anisotropy.

For $\varepsilon_{FP}/u=-3$, namely, when the folded, FP, shapes are intrinsically much more probable than the extended shapes (EA and L), the SmA_{d2} molecular organization dominates the layered mesophases except for a small window at high pressures-low temperatures where the SmAd_1 phase is more stable, [Fig. 5(a)]. In this case the nematic phase appears only at very low temperatures. On increasing the free energy ε_{FP} but still keeping it negative, $\varepsilon_{FP}/u=-1$, the overall topology of the phase diagram remains the same but with a larger SmA_{d1} phase region [Fig. 5(b)]. The tendency towards the stabilization of a SmA_{d1} type of molecular organization is further strengthened when $\varepsilon_{FP}/u=1$ [Fig. 5(c)]. In that case, with the folded parallel shape having higher intrinsic free energy (lower probability) than the extended antiparallel shape, the SmA_{d1} window extends to higher temperatures. For the cases mentioned above there are three possibilities of phase sequences on decreasing the temperature at constant pressure: (a) the high-pressure phase sequence I-SmA_{d1}-SmA_{d2}, (b) the intermediate pressure sequence I-SmA_{d2}, and (c) the low-pressure sequence I-N-SmA_{d2}.

The topology of the phase diagram and subsequently the possible phase sequences change dramatically when $\varepsilon_{FP}/u=3$ [Fig. 5(d)]. In that case the region of stability for the SmA_{d1} is greatly enhanced covering, for moderate pressures, the entire temperature range. Thus the phase sequences I-SmA_{d1} and I-N-SmA_{d1}, not observed before, become possible when the molecular shapes with their branches separated (EA or L shapes) are given high intrinsic probabilities.

Near the smectic-smectic phase transitions the spacing of the layered phases increases significantly. This is found not to be due to a weakening of the molecular interdigitation but rather to the formation of thermodynamicaly stable incommensurate smectic phases with the layers divided into sublayers exhibiting both SmA_{d1} and SmA_{d2} types of molecular organization. These intermediate phases are stable over very narrow ranges, appearing in a nearly continuous succession between SmA_{d1} and SmA_{d2}.

The molecular organization in the smectic phases and the relative population of the shapes are dictated mainly by microsegregation. This is demonstrated in Fig. 6 where we have plotted the bulk probability of the three molecular shapes as a function of pressure at a fixed value of the scaled temperature $u/k_BT=0.20$ for the system with $\varepsilon_{FP}/u=-1$. On the same diagram, the horizontal lines indicate the intrinsic probability of the EA shape and the L shape (solid line) and the FP shape (dashed line). It is clear from this plot that the L shape becomes substantially less probable in all ordered phases while it is equally probable with the EA shape in the isotropic phase. The marked changes of the bulk probabilities across the phase transitions reveal the conformational nature of the transitions. It is worth noting that these bulk probabilities can be viewed as the relative concentrations in a "mixture" of the three shapes that is optimized with respect to their packing in each of the thermodynamically stable phases. The interconverting shape approach used here provides precisely the basis for the self-consistent determination

of the stable phases and for the calculation of the "optimal concentrations" of the different shapes as a function of the thermodynamic variables of the system.

We have repeated the calculations retaining only the two linear shapes (EA and FP) and omitting the L shape. In this case, apart from a relatively weak stabilization of the ordered phases with respect to the isotropic phase, the phase diagrams are qualitatively the same with those obtained by retaining all three shapes. This demonstrates that molecular shapes whose symmetries deviate significantly from the symmetry of the phase have a minor influence on the molecular organization in the ordered phases, since they are strongly suppressed within the bulk phase, even though their intrinsic probability is comparable to that of the dominant shapes.

We have also investigated the TMB systems in the presence of intrinsically directional block-block interactions for the end blocks, which correspond to mesogenic units. We have considered orientational interactions whose relative strength $\tilde{w}^{(0)}_{m,m} \equiv w^{(0)}_{m,m}/u$ with respect to the isotropic interaction is varied from $\tilde{w}^{(0)}_{m,m}=-0.5$ up to -2. The calculated phase diagrams are presented in Figs. 7(a)–7(c). It is apparent from the graphs that the topology of the phase diagrams presents some clear differences from the corresponding phase diagrams of the systems that lack orientational interactions. Thus, when the strength of the orientational interaction is quite high the nematic phase disappears completely from the phase sequence in favor of the smectic phase (Fig. 7(c)). This implies that the directional interactions of the end blocks strengthen the molecular tendency for microsegregation. A notable consequence of the directional interactions on the layered molecular organization is the lowering of the degree of interdigitation. This happens because molecules of adjacent layers interdigitate only up to the extent that their mesogenic end blocks are brought to side-by-side register. This picture is consistent with the destabilization of the $\mathrm{Sm}A_{d1}$ on increasing the strength of the orientational interactions due to the fact that the $\mathrm{Sm}A_{d2}$-like molecular organization allows on average more registered end blocks per layer compared to the $\mathrm{Sm}A_{d1}$-like molecular organization.

Turning now to the twin TDB-C_{60} systems, we show in Figs. 8(a)–8(d) the phase diagrams of pressure versus intrinsic probability of the extended antiparallel shape, for four different values of the interaction parameter u/k_BT.

The phase diagram in Fig. 8(a) has been calculated for $u/k_BT=0.025$, corresponding to weakly repulsive addends. The system exhibits two smectic-A phases of which the high-pressure/low-temperature phase is a $\mathrm{Sm}A_{d1}$ (fullerene monolayer) and the low pressure is a $\mathrm{Sm}A_{d2}$ (fullerene bilayer). The stability of the phases is due to the microsegregation dictated by the molecular partitioning. As seen in Fig. 8(b), increasing the strength of the interblock repulsion to $u/k_BT=0.05$ yields a phase diagram that differs from that of Fig. 8(a) in that the $\mathrm{Sm}A_{d2}$ phase is stable over a narrower pressure range and a small nematic region appears between the isotropic and the $\mathrm{Sm}A_{d2}$ regions at high intrinsic probabilities of the extended antiparallel shape.

For $u/k_BT=0.1$ we have significant changes in the phase diagram, shown in Fig. 8(c), with respect to the phase diagrams obtained with weaker interactions [Figs. 8(a) and 8(b)]. First, the structure of the low-pressure smectic phase is no more interdigitated: the layer spacing becomes equal to the full length of the extended antiparallel molecular state. Secondly, the interdigitated $\mathrm{Sm}A_{d1}$ phase appears only at high pressures and is strongly destabilized at high intrinsic probability of the extended antiparallel shape. Lastly, the nematic range is significantly broadened. These differences indicate that strengthening the repulsive interactions between the addend blocks enhances the role of the overall molecular shape in driving the molecular self-organization and weakens the influence of submolecular partitioning, therefore rendering less significant the contribution of the microsegregation mechanism to the molecular ordering. These inferences are further supported by the phase behavior of the system for $u/k_BT=0.2$. As indicated on the phase diagram in Fig. 8(d), this system does not exhibit any interdigitated smectic phases. The possible phase sequences are either I-SmA, at low intrinsic probability of the extended antiparallel shape,

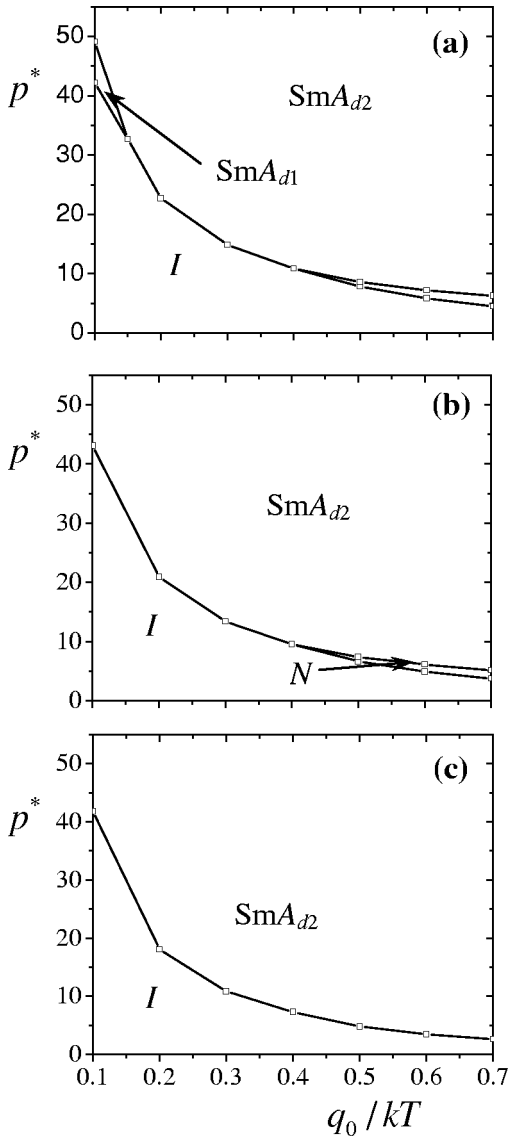

FIG. 7. Same as in Fig. 5(b) only with the end blocks (mesogenic units) interacting via an additional directional component of the potential whose strength $\tilde{w}^{(0)}_{m,m}$ relative to that of the nondirectional component u is given by (a) $\tilde{w}^{(0)}_{m,m}=-0.5$, (b) $\tilde{w}^{(0)}_{m,m}=-1$, and (c) $\tilde{w}^{(0)}_{m,m}=-2$.

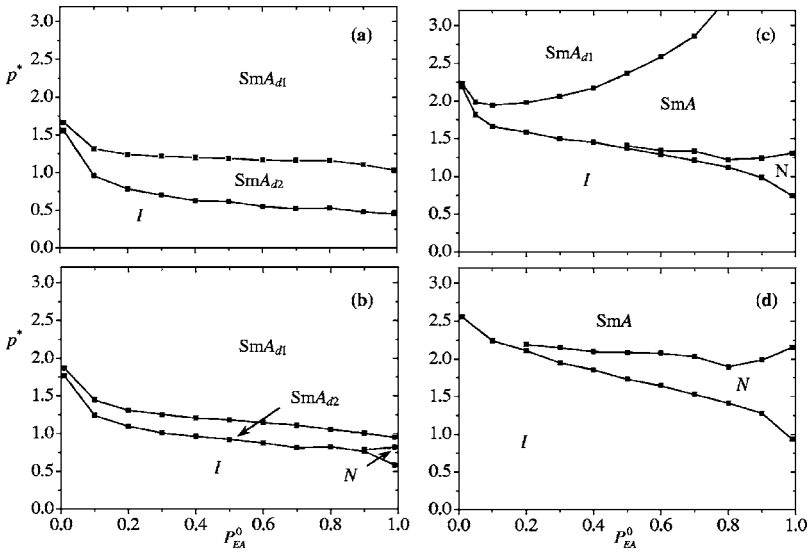

FIG. 8. Calculated p^*, P^0_{EA} phase diagrams (dimensionless pressure vs intrinsic probability of the EA shape) for the TDB-C_{60} monoadducts for four different values of the interaction parameter u/k_BT: (a) 0.025, (b) 0.05, (c) 0.1, and (d) 0.2, respectively.

or *I*-*N*-Sm*A*, at higher probabilities. These are similar to the phase sequences exhibited by sterically interacting rodlike systems.[27]

Generally, in the limit of very low intrinsic probability for the EA shape, namely, when $P^0_{\mathrm{EA}} \ll 1$ for the TDB model systems or when $\varepsilon_{\mathrm{FP}} \ll \varepsilon_{\mathrm{EA}}$ for the TMB, the molecules are practically rigid, exhibiting a single shape with the mesogenic units extended on the same side. Clearly, these molecular shapes are comparable to the dominant shapes of the single dendromesogenic branch monoadducts of C_{60} shown schematically in Fig. 1(c). These systems do not exhibit nematic phases indicating that enhanced molecular polarity disfavors nematic ordering. This is in accordance with what is observed experimentally.[7,8,13] Furthermore, the molecular organization within the smectic layers corresponds to a bilayer arrangement with a spacing of about six submolecular blocks. Taking into account that the block length is roughly 9 Å (the fullerene diameter), the calculated spacing is found around 55 Å, in good agreement with x-ray-diffraction (XRD) measurements on the real compounds.[7]

When all the shapes come into play the phase behavior becomes richer, primarily due to the formation of various smectic phases. The polymorphism of the smectic organization stems from chemical affinity differences between distinct molecular parts in conjunction with molecular flexibility. Thus, the degree of interdigitation between adjacent layers and the molecular organization within the layers are determined by the interplay between the molecular flexibility and the formation of well-defined microsegregated structures. As calculations indicate, phase transitions between smectic phases are accompanied by rather strong conformational changes but not necessarily by substantial changes of the layer spacing. Regarding the smectic phases of the studied TMB and TDB systems, the SmA_{d2} phase is favored primarily by the high probability of the FP shapes while the SmA_{d1} is more stable when the EA molecular shapes have appreciable intrinsic probability. Both phases exhibit extended interdigitation and their layer spacing differs by one fullerene diameter (9 Å).

Finally, for the conical supermesogens with a fullerene apex (CSM-C_{60}), the assumed effective rigidity of the block representation of the molecule removes any dependence of the phase behavior on the conformational statistics. The block-block interaction potential used for the CSM-C_{60} calculations is formulated and parametrized along the same lines described for TMB-C_{60}, and TDB-C_{60} with $u^{(0)}_{f,f}=u^{(0)}_{f,m}=\infty$, $u^{(0)}_{m,m}=u>0$, $u^{(1)}_{i,j}=0$, and no *l* blocks present. Here, as before, u is a measure of the softness of the repulsions among the grafted addends. Figure 9 shows the calculated phase diagram, the thermodynamic variables in this case being the scaled pressure, $p\nu_{\mathrm{mol}}/u$, and the scaled reciprocal temperature u/k_BT. It is apparent on that phase diagram that the system, depending on pressure, may exhibit two different phase sequences. At low pressures the system transforms, on lowering the temperature, from the isotropic phase to a columnar phase through a first-order transition. At higher pressures, a bilayer interdigitated smectic-*A* phase is inserted between the isotropic and the columnar phase.

Strictly, the positional organization of the CSM-C_{60} supermesogens in the plane perpendicular to the columns is forced to a rectangular columnar ordering due to the imposed cubic lattice restrictions on the positions of submolecular blocks. In other words, the axis parallel to the common column orientations can only be a C4 or a C2 symmetry axis and therefore the only two-dimensional positional order al-

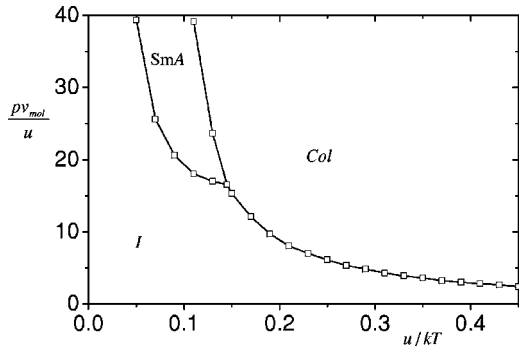

FIG. 9. Calculated phase diagram for CSM-C_{60} conical molecules with a fullerene apex.

lowed is of rectangular symmetry. This makes it impossible to distinguish between hexagonal and rectangular columnar phases within the present lattice model. However, the phase behavior of the system, in particular, the phase boundaries of the columnar phase to the isotropic or to the smectic phase, is not expected to be severely influenced by this limitation since the free-energy difference between a hexagonal and rectangular columnar phases is expected to be rather low compared to the difference between the columnar (rectangular or hexagonal) and nematic or smectic free energy.

The picture for the *intracolumnar* organization of the CSM-C_{60} supermesogens is clear: the columns are strongly polar since the molecules stack one on the top of the other so that the fullerene unit of the upper molecule is accommodated inside the cone aperture formed by the addends of the next supermesogen in the column. It should be noted here that, as a consequence of assuming nonpolar block-block interactions, the energy required to slide two adjacent columns parallel to each other does not depend on the their polarity. Accordingly, the overall polarity of these columnar phases is determined solely on entropic grounds, rendering the macroscopically apolar columnar phases more stable than the polar ones.

IV. CONCLUSIONS

We have studied the phase behavior and the molecular organization for a wide variety of fullerene containing liquid crystals with the aid of a simple molecular theory. Despite the very crude representation of the molecular structure in terms of a small number of submolecular blocks, restricted to move on a cubic lattice and interacting via simplified additive block-block potentials, the theory accounts consistently and qualitatively for the basic experimental observations on all the classes of compounds considered. The observed nematic, smectic, and columnar phases are reproduced correctly and the molecular features that influence their stability are identified. The peculiar smectic polymorphism exhibited by compounds of twin-branch architecture is elucidated in relation to molecular structure and interactions. While the molecular modeling and the computational aspects of the theory are susceptible to further refinements, the results obtained with its present, simplified, form can be useful for the molecular design of model fullerene-containing liquid-crystalline compounds.

ACKNOWLEDGMENTS

One of the authors (S.D.P.) acknowledges funding from the European Social Fund (ESF), Operational Program for Educational and Vocational Training II (EPEAEK II) through the Program IRAKLEITOS. Another author (A.G.V.) acknowledges support through the "Caratheodores" research programme of the University of Patras. Support from the RTN Project "Supermolecular Liquid Crystal Dendrimers-LCDD" (HPRN-CT2000-00016) is also acknowledged.

APPENDIX: OUTLINE OF THE INTERCONVERTING SHAPE APPROACH

Here we summarize the statistical-mechanics foundation of the interconverting shape approach[20] that we have applied to the fullerene-containing supermesogens (here refereed to simply as "molecules") of the present study.

Consider an ensemble of N identical molecules occupying volume V at temperature T. The individual molecules are labeled by the indices $I,J\ldots=1,2,3,\ldots,N$. We denote the position of the Ith molecule by $\mathbf{R}_I$ and its orientation by Ω_I. These variables are denoted collectively by $\omega_I=(\mathbf{R}_I;\Omega_I)$. The set of variables specifying the conformational state of the molecule are denoted by ν_I and $E(\nu_I)$ stands for the energy of the molecule at that state.

It is assumed that the interaction between two such molecules can be described by the pair potential $U_{I,J}=U(\mathbf{R}_{I,J};\Omega_{I,J};\nu_I,\nu_J)$, with $\mathbf{R}_{I,J},\Omega_{I,J}$ denoting, respectively, the position and orientation of molecule J relative to I. Each molecule is taken to consist of a number of effectively rigid segments (or submolecular "blocks") and the interaction potential $U_{I,J}$ is further assumed to be a superposition of potentials among all the *intermolecule* pairs of such segments. Accordingly the interaction potential between molecules I and J is written as

$$U_{I,J}=\sum_{b_I,b_J} u_{b_I,b_J}(\omega_{b_I,b_J}), \tag{A1}$$

where ω_{b_I,b_J} denotes collectively the relative positions $\mathbf{R}_{b_I,b_J}$ and orientations Ω_{b_I,b_J} of the pair of blocks b_I,b_J and the summation runs over all the blocks of molecules I and J.

The conformational energy $E(\nu_I)$ is understood to originate from the interactions among the segments that form molecule I. Assuming for simplicity that the conformational states of the molecule are discreet we may define

$$P_\nu^0 \equiv \frac{e^{-E_\nu/kT}}{\left[\sum_\nu e^{-E_\nu/kT}\right]}, \tag{A2}$$

as the intrinsic probability for the molecule to be found in conformation ν in the absence of any interactions with the other molecules of the ensemble.

A further step of simplification is to assume that the conformational states can be grouped into sets, with the states in each set exhibiting identical molecule-molecule interaction $U_{I,J}=U(S_I,S_J;\omega_{I,J})$. These sets of conformations are referred to as the shapes of the molecules and are denoted by S_I,S_J. The set of distinct conformations associated with the same shape S_I is denoted by $\nu(S_I)$.

The intrinsic probability P_S^0 of the shape S is given by the sum of the intrinsic probabilities of all the conformations that correspond to that shape, i.e.,

$$P_S^0 \equiv \sum_{\nu(S)} P_\nu^0. \tag{A3}$$

The intrinsic energy ε_S of the shape S is defined in terms of the intrinsic probability according to

$$P_S^0 \equiv \frac{e^{-\varepsilon_S/kT}}{\left[\sum_{S'} e^{-\varepsilon_{S'}/kT}\right]}. \tag{A3'}$$

According to Eqs. (A2) and (A3), ε_S is an effective free energy whose relation to the energies E_ν of the conformations forming the set $\nu(S)$ is given by

$$\varepsilon_S = -k_B T \ln \sum_{\nu(S)} e^{-E_\nu/k_B T}. \tag{A3''}$$

The thermodynamic description of the fluid phases is based on the approximate expression for the configurational free energy

$$-F'/Nk_BT \approx \ln\left[\sum_S P_S^0 \int d\omega \zeta_S(\omega)\right] + \frac{1}{2}(N-1)\ln\langle G\rangle, \tag{A4}$$

which is obtained within the variational cluster method on retaining only up to two-molecule cluster terms. In this expression $\zeta_S(\omega)$ is the variational weight function for the shape S. The interaction between a molecule in any conformation of shape S_I with another molecule in any conformation of shape S_J is introduced through the function

$$G_{S_I,S_J}(\omega_{I,J}) \equiv e^{-U(S_I,S_J;\omega_{I,J})/kT}, \tag{A5}$$

where $\omega_{I,J}$ denotes the relative positional and orientational variables $\mathbf{R}_{I,J}, \Omega_{I,J}$ of the molecular pair I,J. The angular brackets in Eq. (A4) indicate ensemble averaging according to

$$\langle G\rangle \equiv \sum_{S_I,S_J} \int d\omega_I d\omega_J \rho_{S_I}(\omega_I)\rho_{S_J}(\omega_J) G_{S_I,S_J}(\omega_{I,J}), \tag{A6}$$

using the single-molecule probability distribution function

$$\rho_S(\omega) = \frac{P_S^0 \zeta_S(\omega)}{\sum_{S'} P_{S'}^0 \int d\omega' \zeta_{S'}(\omega')}. \tag{A7}$$

The variational weight function $\zeta_S(\omega)$ is determined self-consistently by functional minimization of the free energy F' leading to the condition

$$\zeta_S(\omega) = \exp\left[\frac{\langle G_{S_I}(\omega_I)\rangle - \langle G\rangle}{\langle G\rangle}\right], \tag{A8}$$

where

$$\langle G_{S_I}(\omega_I)\rangle = \sum_{S_J} \int d\omega_J \rho_{S_J}(\omega_J) G_{S_I,S_J}(\omega_{I,J}). \tag{A9}$$

The pair distribution function in this approximation is given by

$$\rho^{(2)}_{S_I,S_J}(\omega_I,\omega_J) = \rho_{S_I}(\omega_I)\rho_{S_J}(\omega_J) G_{S_I,S_J}(\omega_{I,J})/\langle G\rangle. \tag{A10}$$

According to Eqs. (A4)–(A10), the equilibrium thermodynamic properties and the molecular statistics within this approximation are completely specified in terms the intrinsic probabilities P_S^0 (or the effective free energies ε_S) of the various molecular shapes and their respective pair interaction functions $G_{S_I,S_J}(\omega_{I,J})$ defined by Eq. (A5). Both, P_S^0 and $G_{S_I,S_J}(\omega_{I,J})$, can be modeled to the required level of resolution by carrying out molecular-mechanics calculations on a single molecule and on a molecular pair, respectively. Naturally, the computational feasibility of this approach rests on the possibility of grouping the (normally quite numerous) molecular conformations into a small number of representative shapes. It should be noted that the important shapes are not necessarily the ones exhibiting high intrinsic probabilities P_S^0 in isolation but rather the ones that acquire high probabilities in the bulk phase of the interacting molecules. These probabilities are given by

$$P_S = \int d\omega \rho_S(\omega) = \frac{P_S^0 \int d\omega \zeta_S(\omega)}{\sum_{S'} P_{S'}^0 \int d\omega' \zeta_{S'}(\omega')}, \tag{A11}$$

and they clearly involve both, the intrinsic probability for the shape S to occur in the absence of intermolecular interactions *and* the average interaction of that shape with its environment in the bulk phase.

The symmetry of the phase is entered in the self-consitency calculations through the assumed dependence of the variational weight function on the positional and orientational variables $\omega=(\mathbf{R};\Omega)$. For the fluid phases of the present study we have the following types of $\zeta_S(\omega)$ functional dependence according to phase symmetry:

- isotropic phases, for which $\zeta_S(\omega)$ is independent of position and orientation,
- nematic phases, for which $\zeta_S(\omega)$ is independent of position,
- smectic phases, for which $\zeta_S(\omega)$ is independent of the positional coordinates in the plane of the smectic layers, and
- columnar phases, for which $\zeta_S(\omega)$ is independent of the positional coordinate along the columnar axis.

The lattice version of this approach merely introduces a further computational simplification by replacing the full position-orientation integrations indicated in Eqs. (A4), (A6), (A7), (A9), and (A11) with summations over lattice points. Clearly, this simplification allows for an analogously coarse grained modeling of the molecular interactions and of the geometry of the molecular shapes.

[1] M. Prato, J. Mater. Chem. **7**, 1097 (1997).
[2] D. M. Guldi, M. Maggini, G. Scorrano, and M. Prato, J. Am. Chem. Soc. **119**, 974 (1997).
[3] E. Peeters, P. A. van Hal, J. Knol, C. J. Brabec, N. S. Sariciftci, J. C. Hummelen, and R. A. J. Janssen, J. Phys. Chem. B **104**, 10174 (2000).
[4] M. Even, B. Heinrich, D. Guillon, D. M. Guldi, M. Prato, and R. Deschenaux, Chem.-Eur. J. **7**, 2595 (2001).
[5] T. Chuard and R. Deschenaux, Helv. Chim. Acta **79**, 736 (1996).
[6] T. Chuard, B. Dardel, R. Deschenaux, and M. Even, Carbon **38**, 1573 (2000).
[7] B. Dardel, D. Guillon, B. Heinrich, and R. Deschenaux, J. Mater. Chem. **11**, 2814 (2001).
[8] T. Chuard and R. Deschenaux, J. Mater. Chem. **12**, 1944 (2002).

[9] R. Deschenaux, M. Even, and D. Guillon, Chem. Commun. (Cambridge) **5**, 537 (1998).
[10] B. Dardel, R. Deschenaux, M. Even, and E. Serrano, Macromolecules **32**, 5193 (1999).
[11] N. P. Yevlampieva, B. Dardel, P. Lavrenko, and R. Deschenaux, Chem. Phys. Lett. **382**, 32 (2003).
[12] S. Campidelli, C. Eng, M. I. Saez, J. W. Goodby, and R. Deschenaux, Chem. Commun. (Cambridge) **13**, 1520 (2003).
[13] S. Campidelli and R. Deschenaux, Helv. Chim. Acta **84**, 589 (2001).
[14] S. Campidelli, R. Deschenaux, J. F. Eckert, D. Guillon, and J-F. Nierengarten, Chem. Commun. (Cambridge) **6**, 656 (2002).
[15] N. Tirelli, F. Cardullo, T. Habicher, U. W. Suter, and F. Diederich, J. Chem. Soc., Perkin Trans. 2 **2**, 193 (2000).
[16] T. Chuard, R. Deschenaux, A. Hirsch, and H. Schönberger, Chem. Commun. (Cambridge) **20**, 2103 (1999).
[17] C. Tschierske, Nature (London) **419**, 681 (2002).
[18] M. Sawamura, K. Kawai, Y. Matsuo, K. Kanie, T. Kato, and E. Nakamura, Nature (London) **419**, 702 (2002).
[19] Y. Matsuo, A. Muramatsu, R. Hamasaki, N. Mizoshita, T. Kato, and E. Nakamura, J. Am. Chem. Soc. **126**, 432 (2004).
[20] A. G. Vanakaras and D. J. Photinos, J. Mater. Chem. **15**, 2002 (2005).
[21] A. G. Vanakaras and D. J. Photinos, Mol. Phys. **85**, 1089 (1995).
[22] R. Berardi, S. Orlandi, D. J. Photinos, A. G. Vanakaras, and C. Zannoni, Phys. Chem. Chem. Phys. **4**, 770 (2002).
[23] MATERIALS STUDIO™ (Accelrys Inc., Cambridge, 2002).
[24] F. Hardouin, A. M. Levelut, M. F. Archad, and G. Sigaud, J. Chim. Phys. Phys.-Chim. Biol. **80**, 53 (1983).
[25] J. W. Goodby and G. W. Gray, in *Physical Properties of Liquid Crystals*, edited by G. W. Gray, V. Vill, H. W. Spiess, D. Demus, and J. W. Goodby (Wiley-VCH, Weinheim, 1999), Chap. 2, pp. 17–24.
[26] P. Barois, Phys. Rev. A **33**, 3632 (1986).
[27] S. C. McGrother, D. C. Williamson, and G. Jackson, J. Chem. Phys. **104**, 6755 (1996).